Reconfigurable Graphene-Based Metamaterial Polarization Converter for Terahertz Applications

Ahmed Mosaad Mabrouk (ahmed.mosaad@buc.edu.eg)
Badr University in Cairo https://orcid.org/0000-0001-5598-7349
A. A. Donkol
NUB: Nahda University
Asmaa G. Seliem
NUB: Nahda University

Research Article

Keywords: Graphene, Metamaterial, Polarization Converter, Axial Ratio, THz

Posted Date: March 22nd, 2022

DOI: https://doi.org/10.21203/rs.3.rs-1268840/v1

Reconfigurable Graphene-Based Metamaterial Polarization Converter for Terahertz Applications

A. M. Mabrouk[1*], A. A. Donkol[2] , and Asmaa. G. Seliem[3]
[1]*Faculty of Engineering and Technology, Badr University in Cairo (BUC), Egypt.*
[2]*Faculty of Engineering, Nahda University in Benisuif (NUB), Egypt E-mail: eng_ahmeddonkol@yahoo.com.*
[3]*Faculty of Engineering, Nahda University in Benisuif (NUB), Egypt E-mail:asmaa.seliem@s-mu.edu.eg*
* Corresponding author *E-mail: *ahmed.mosaad@buc.edu.eg*

Abstract

This paper suggests a high gain polarization converter using a graphene-based metamaterial array. The graphene-based metamaterial polarization converter is a rectangular array that consists of 20 periodic unit-cell elements. Each graphene-based metamaterial unit-cell element consists of a rectangular patch with four triangular-shaped graphene parts at its four corners. The rectangular patch with the four graphene parts are placed over a rectangular substrate backed with a perfect electric conductor (PEC) and has a relative permittivity of ε_{sub}= 3.38. The metamaterial characteristics of the proposed graphene-based metamaterial unit-cell element are obtained over a wide range of frequencies of 0.7 THz ranging from 1.5 THz to 2.2 THz. The graphene-based metamaterial array is placed over a linear polarized slot antenna that operates at 1.8 THz with a maximum gain of 5.5 dBi. The linearly polarized wave that radiated from the slot antenna can be converted into a reconfigurable right-handed circular polarization (RHCP) or Left-handed circular polarization (LHCP) according to the biasing states of the graphene parts. Moreover, the operating -10 dB B.W of the slot antenna is increased to 22.2 %, and the gain is enhanced to 8 dBi at the same operating frequency. A reconfigurable polarization conversion for the slot antenna can be obtained over a wide 3dB axial ratio (AR) B.W from 1.75 THz to 1.92 THz (20 % 3dB B. W).

Keywords: *Graphene, Metamaterial, Polarization Converter, Axial Ratio, THz*

I. Introduction

Terahertz waves in recent years are used for many applications. In medical, THz radiation can also detect differences in water content and density of a tissue. THz waves are used in airports for security to detect hidden illegal substances with passengers. In Communication, because of their higher carriers' frequency, higher data rates are achieved (up to 1000's Gbit/s data rates). In manufacturing processes, THz waves are used for imaging and sensing, quality control, and monitoring [1]. Metals like copper and gold are used for antenna applications in this band [2]. Copper is the most used metal for antenna applications in the THz band [3]. But the copper-based antennas suffer from high propagation losses and low radiation efficiency at that band of frequencies. These disadvantages exist as the conductivity, and the skin depth of the copper metal are decreased in the THz band. These facts encourage the usage of carbon-based materials, such as graphene and carbon nanotubes (CNT) for THz antennas. Graphene is defined as a two-dimensional carbon membrane with a thickness of one atom arranged in a single or multiple layers [4]. Graphene material has unique characteristics rather than other materials. It has high electron mobility that at room temperature approaches 20 m^2/V. s. Graphene, compared to the materials ever discovers, is the strongest because of its lattice configuration. Graphene's breaking strength is 100 times the steel's breaking strength. Graphene is the stiffest material ever studied, and it has mechanical stress of 100 GN/m^2 (1×10^{11} N/m^2) and an elastic modulus of 1 TN/m^2 (1×10^{12} N/m^2) [5]. Although the highest mechanical properties, graphene material has impressive flexibility [6]. Reconfigurability of the antenna's properties has attracted the attention of researchers in the field of wireless communications, especially mobile and satellite [7-10]. The most popular antenna properties that can be reconfigurable are the operating frequencies, the radiation pattern, and the polarization [11], [12]. The budget of the propagation link is mainly affected due to polarization mismatch at the receiving side in most wireless communication applications. Verifying that the linearly

polarized (LP) wave in satellite communication may be rotated while transferring between the transmitting and receiving sides. The rotation of the LP wave is named Faraday rotation which increases the budget of the propagation link [13]. This issue decreases the usage of LP waves in wireless applications. Also, from the drawbacks of LP waves multipath fading during transmission and the orientation of the antenna at the receiving side. So, the need for using circularly polarized waves became a necessity because of its advantages compared to the LP waves [14-16]. The most important advantage of the CP is its high immunity against the transmission medium effects [17-19]. To convert the LP wave to CP wave, the researchers started to design an aided construction that can obey that conversion which is called polarization converters. The antenna that can perform such conversion is called a reconfigurable polarization antenna [20]. Reconfigurable polarization means the ability of the antenna to switch between LP to left-hand circular polarization (LHCP) or right-hand circular polarization (RHCP) or between LHCP and RHCP, this property solved the single polarization issue in the antenna field [21]. Different structures can be used to convert the LP wave from the antenna to the CP wave. These surfaces may be designed based on artificial magnetic conductors (AMC) [22] or frequency selective surfaces [23]. Other surfaces are based on metamaterials (MM) which are defined as artificial structures that have a negative real part of electrical permittivity (ε), a negative part of magnetic permeability (μ), and a negative real part of refractive index (n) at the operating frequency of the antenna [24]. The MM surfaces are designed as a periodic structure from the unit-cell elements that satisfy the electromagnetic properties (ε, μ, and n) of the metamaterials. The operating frequency of the MM surfaces can be tuned geometrically by changing the dimensions of one/all constituent parts of the unit-cell element that result in changing its conductance and capacitance [25]. The performance of the MM unit-cell elements can be changed electrically, thermally, chemically, or optically according to the type of materials used in the proposed design [26]. It can also be changed using positive intrinsic negative (PIN) diodes, varactor diodes, or microelectromechanical systems (MEMS) [27].

In this article, a graphene-based MM (GMM) unit-cell element is designed at the operating frequency of 1.8 THz. The GMM properties (ε, μ, and n) and the 3-dB axial ratio (AR) are calculated and figured. This unit-cell element is then arranged in an MM-based surface that is used to obtain a reconfigurable polarization dipole antenna in the Terahertz (THz) band. A 4 x 4 GMM-based array is used as a reflector for the proposed dipole antenna to convert its LP wave to LHCP or RHCP through the biasing state of each two opposite graphene triangles. The proposed constructions are designed and analyzed using computer simulation technology microwave studio (CST-MW) that is based on finite integration technique (FIT). Section-II presents the design and analysis of the GMM-based unit-cell element. In section-III, the design and analysis of the reconfigurable polarization slot antenna are introduced. Section-V concludes this paper.

II. Design And Analysis of Graphene-Based Metamaterial Unit-Cell Element

The GMM-based unit-cell element consists of a rectangular copper patch of a side length (L_P = 26.84 µm) with four triangular-shaped graphene parts at its coroners. Each graphene triangle has two equal sides of length (a = 10.93 µm) and base of length (b = 15.46 µm) as shown in Fig. 1. Two of them are placed oppositely at an angle of 45° and the other two are placed at an angle of - 45° concerning the positive x-axis. The copper patch and the four graphene triangles are placed over a square-shaped substrate of side length (L_S = 29.82 µm), the height of (H_S = 7.57 µm), and relative permittivity (ε_{rsub} = 3.38), which is backed by a square perfect electric conductor (PEC) ground plane of the same side length.

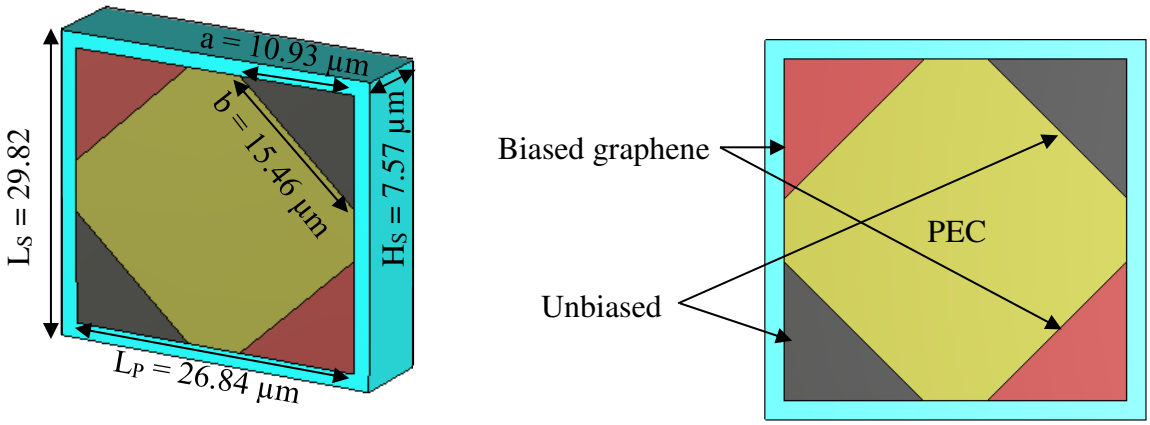

Figure 1. The 3D diagram of the graphene-based metamaterial unit-cell element

Graphene's controllable conductivity (σ(ω)) is the most important property for antenna reconfigurability applications. Dislike most popular materials, graphene conductivity can be altered in different ways, such as applied electric field, applied DC voltage, or chemical doping. Kubo formula represents the graphene conductivity as a frequency-dependent complex value according to the following equation [28]:

$$\sigma(\omega) = \sigma_{inter}(\omega) + \sigma_{intra}(\omega) \tag{1}$$

where, $\sigma_{inter}(\omega)$ is the inter-band contribution which corresponds to the generation of electron-hole pair and the events of recombination, and $\sigma_{intra}(\omega)$ is the intra-band contribution which corresponds to the conductivity of free carriers. Each of the inter-band and intra-band is represented as follow:

$$\sigma_{inter}(\omega, \mu_c, \Gamma, T) \approx j\frac{q_e^2}{4\pi\hbar}\, ln\left(\frac{2|\mu_c| - (\omega + j\tau^{-1})\hbar}{2|\mu_c| + (\omega + j\tau^{-1})\hbar}\right) \tag{2}$$

$$\sigma_{intra}(\omega, \mu_c, \Gamma, T) \approx -j\frac{q_e^2\, K_B\, T}{\pi\, \hbar^2\, (\omega - j2\Gamma)} \times \left(\frac{\mu_c}{K_B\, T} + ln(e^{-\mu_c/\, K_B\, T} + 1)^2\right) \tag{3}$$

where ω is the angular frequency, μ_c is the chemical potential (varies between 0 and 2 eV), Γ is the rate of scattering ($\Gamma = 1/\tau$), T is the temperature in Kelvin, τ is the time of relaxation, q_e is the electron charge, K_B is the Boltzmann' s constant, and $\hbar$ is the reduced Plank's constant.

For the operating frequencies below 8 THz, the graphene conductivity can be represented in terms of the inter-band only where the inter-band can be neglected [28]. The most well-known technique used to control the graphene conductivity is through varying the applied DC voltage [29]. In this article we apply the inter-band of the graphene conductivity as it designed for the applications below 8 THz. According to Eq. 2, the graphene acts as a dielectric if it biased with the value of DC voltage equivalent to $\mu_c = 0$ (unbiased state). But it acts as a conductor if it biased with the value of DC voltage equivalent to $\mu_c = 2\ eV$ (unbiased state). In this article we deal with the biased and the unbiased states of graphene to achieve the polarization conversion property as discussed below.

Using a Floquet port in the CST-MW software, the dimensions of the unit-cell element are optimized and analysed. When the two opposite graphene triangles directed to θ_1 = +45° are biased and those that directed to θ_1 = -45° are unbiased (case1), the magnitudes of reflection (S_{11} or T_{xx}) and transmission (S_{21} or T_{xy}) coefficients of the GMM unit-cell element are calculated and figured in Fig. 2. a. The opposite case when the two opposite graphene triangles directed to θ_2 = -45° are biased and those that directed to θ_2 = +45° are unbiased (case 2). The magnitudes of reflection (S_{11} or T_{xx}) and transmission (S_{21} or T_{xy})

coefficients of the GMM unit-cell element are calculated and figured in Fig. 2. b. It can be noted that both T_{xx} and T_{xy} have the same value at a frequency of 1.8 THz. The variation of the reflection (P_{11}) and the transmission (P_{21}) phases and their differences of the two cases are introduced in Fig. 3. From the obtained results, the phase difference in both cases is ($\varphi = 90^o$) at the operating frequency. Form the obtained results, the proposed GMM unit-cell element satisfies the AMC requirements at the operating frequency of 1.8 THz [30].

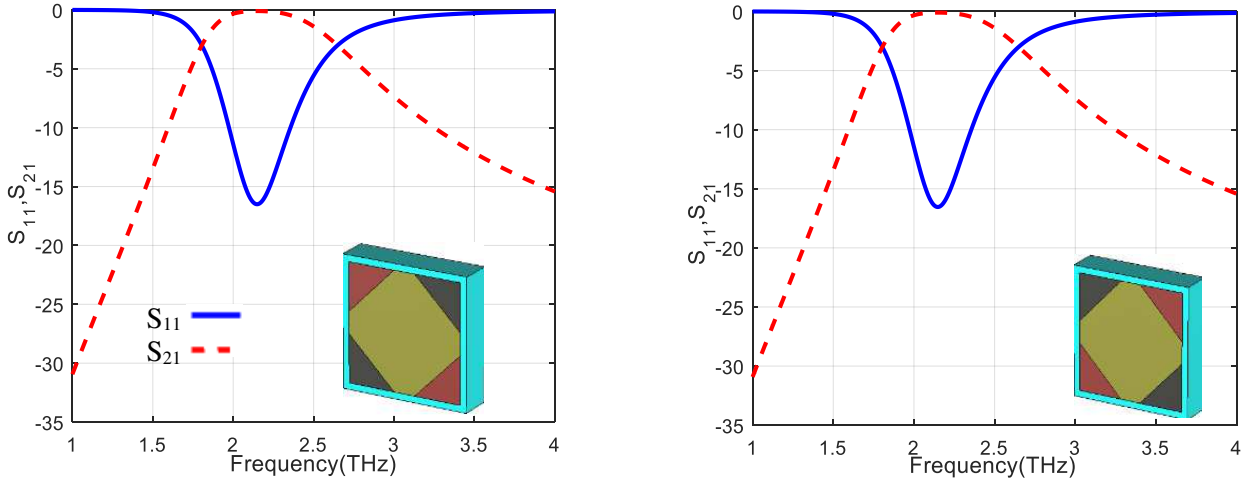

a. b.

Figure 2. The variations of the reflection and transmission coefficients versus frequency of the GMM unit-cell element when (a) the two opposite graphene triangles directed to $\theta_1 = +45^o$ are biased and (b) the two opposite graphene triangles directed to $\theta_2 = -45^o$ are biased.

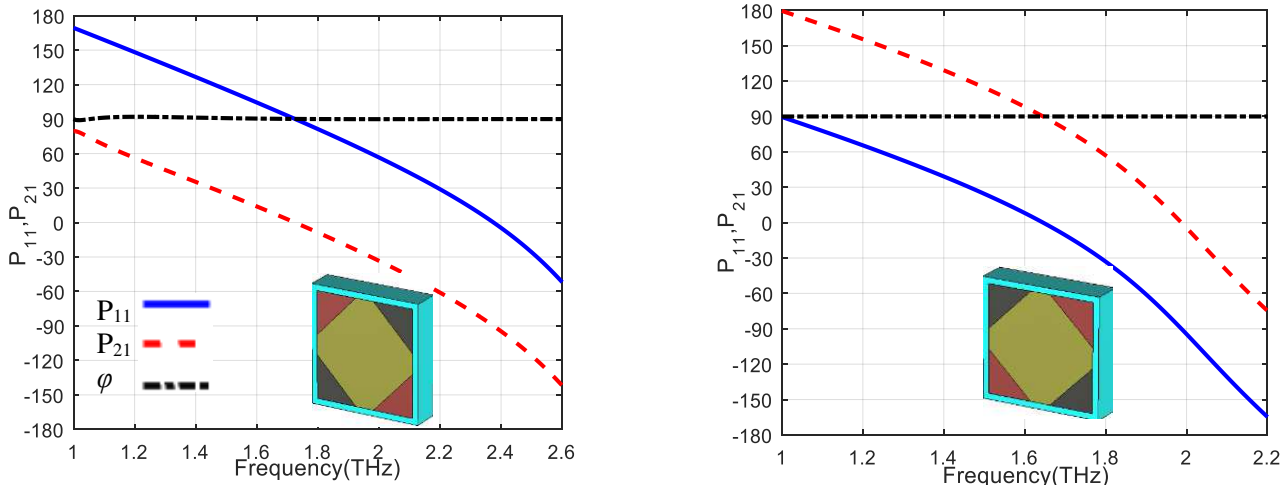

a. b.

Figure 3. The variations of the reflection and transmission phases and their difference versus frequency of the MM unit-cell element when (a) the two opposite graphene triangles directed to $\theta_1 = +45^o$ are biased and (b) the two opposite graphene triangles directed to $\theta_2 = -45^o$ are biased.

The reflection T_{xx} and transmission T_{xy} coefficients are then used to calculate the MM parameters (ε, μ, and n) for the unit-cell element. At first, the impedance z and the refractive index n are calculated using Eq. 3 and Eq. 4, respectively [24]:

$$z = \pm\sqrt{\frac{(1+T_{xx})^2 - T_{xy}{}^2}{(1-T_{xx})^2 - T_{xy}{}^2}} \qquad (3)$$

$$n = \frac{1}{kH}\cos^{-1}\left[\frac{1}{2T_{xy}}(1 - {T_{xx}}^2 + {T_{xy}}^2)\right] \quad (4)$$

Where n is the refractive index, k is the wavenumber of the incident wave, and H is the overall thickness of the metamaterial unit-cell element. These two equations are then used to calculate the electrical permittivity, ε, and the magnetic permeability μ as in Eq. 4 and Eq. 6 respectively [26]:

$$\varepsilon = {}^{n}/_{Z} \quad (5)$$

$$\mu = n \times z \quad (6)$$

The variations of real and imaginary parts of the unit-cell element's parameters (ε, μ, and n) versus frequency are figured in Fig. 4, 5, and 6, respectively. The real parts of ε, μ, and n of the MM unit-cell elements must be negative at the operating frequency which is 1.8 THz in this work. From the results shown in Fig. 4. a, the real part of the relative permittivity ε has negative values through a wide band of frequencies ranging from 1.5 THz to 2.2 THz for case 1 and ranging from 1.6 THz to 2.1 THz for case 2.

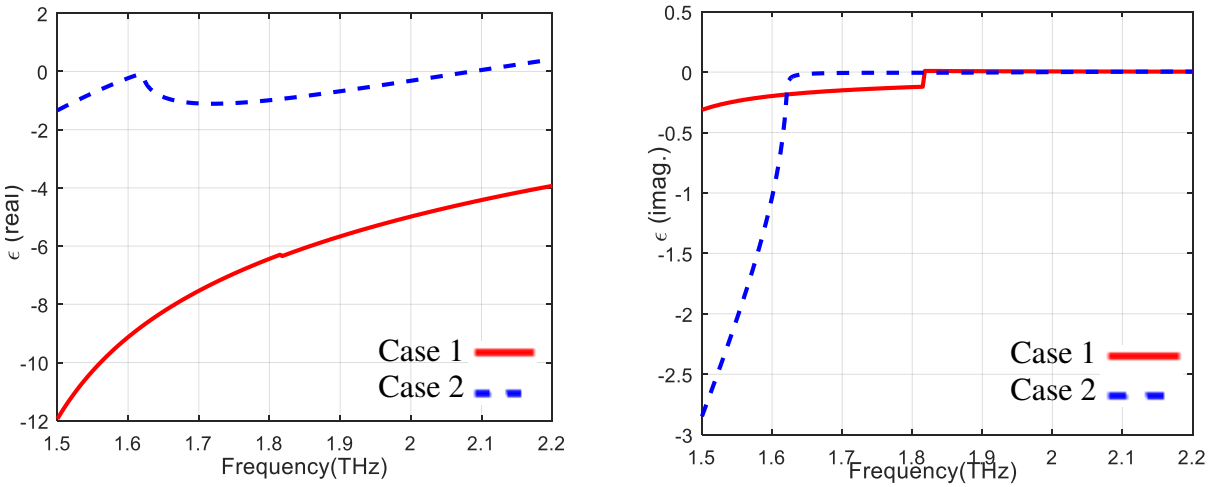

a. b.

Figure 4. The variations of (a) the real part (b) the imaginary part of the permittivity versus frequency of the GMM unit-cell element for case 1 and case 2 respectively.

The real part of the relative magnetic permeability μ has negative values over the frequency band ranging from 1.5 THz to 2.2 THz for case 1 and ranging from 1.6 THz to 2.2 THz for case 2 as shown in Fig. 5. a.

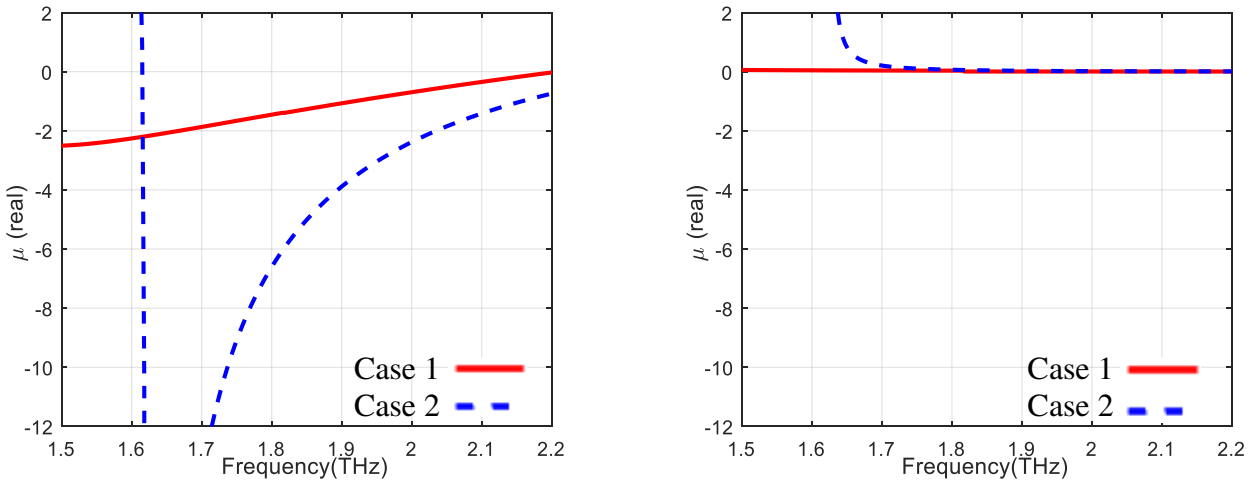

a. b.

Figure 5. The variations of (a) the real part (b) the imaginary part of the permittivity versus frequency of the GMM unit-cell element for case 1 and case 2 respectively.

Also, the proposed GMM unit-cell element has negative values of the refractive index n through the frequency band ranging from 1.6 THz to 2.2 THz for case 1 and case 2 as shown in Fig. 6. a. Here; the proposed unit-cell element is valid to be a MM unit-cell.

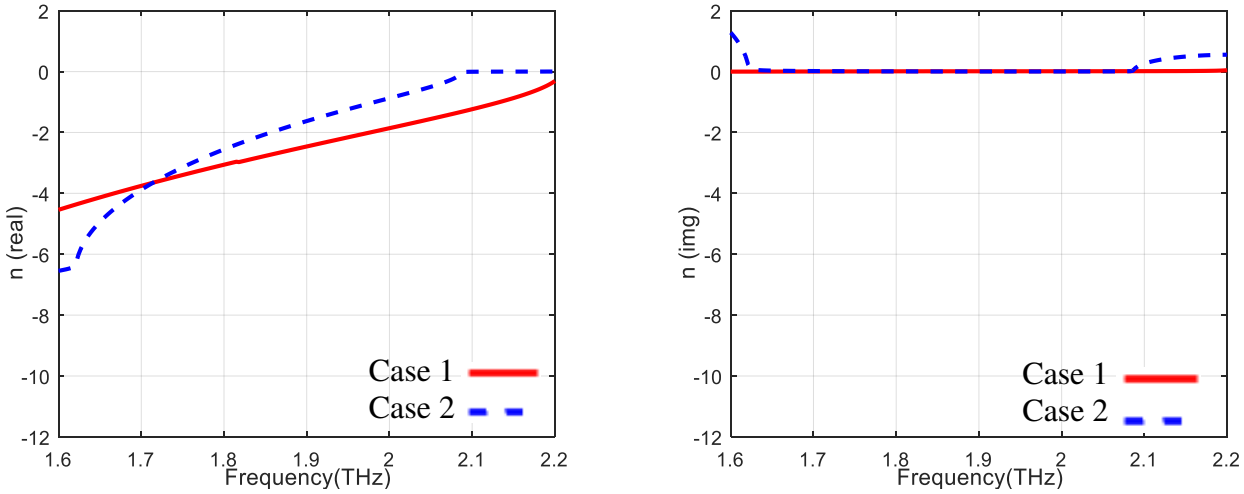

a. b.

Figure 6. The variations of (a) the real part (b) the imaginary part of the refractive index versus frequency of the GMM unit-cell element for case 1 and case 2.

According to the obtained results, the proposed GMM unit-cell element can be used for polarization conversion at 1.8 THz. At that frequency: for the case 1, as the reflection phase P_{11} is greater than that of the transmission phase P_{21} by 90° as shown in Fig. 3. a, the polarization of the transmitted wave is RHCP. For case 2, as the transmitted phase P_{21} is greater than that of the reflection phase P_{11} by 90° as shown in Fig. 3. b, the polarization of the transmitted wave is LHCP [29].

In summary, the proposed GMM unit-cell element is used to convert the incident LP to RHCP or LHCP according to the biasing state of the graphene triangles as in case 1 and case 2. The 3dB AR bandwidth (BW) from 1.78 THz to 1.86 THz (4.4 % 3dB-BW) is achieved for case 1 as shown in Fig. 7. a. The 3dB AR bandwidth (BW) from 1.76 THz to 1.84 THz (4.44 % 3dB-BW) is achieved for case 2 as presented in Fig. 7. b. The AR is calculated and figured out using Eq. 7 [30]:

$$AR = \sqrt{\frac{1+\beta^2+\sqrt{(1-\beta^2)^2+4\beta^2 cos^2\varphi}}{1+\beta^2-\sqrt{(1-\beta^2)^2+4\beta^2 cos^2\varphi}}} \quad (7)$$

Where $\beta = \frac{|T_{xx}|}{|T_{xy}|}$, and φ is the phase difference between T_{xx} and T_{xy}.

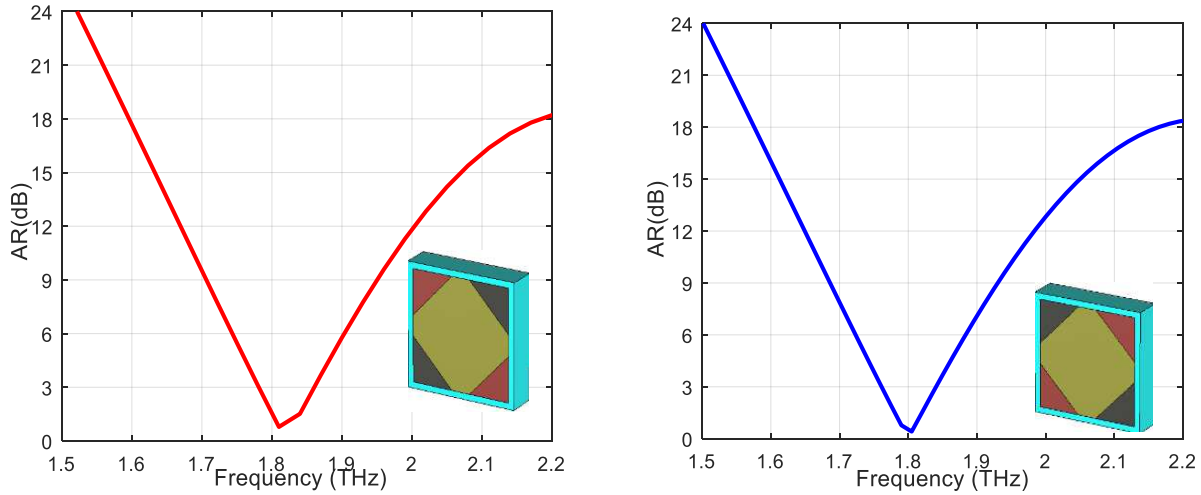

a. b.

Figure 7. The variations of the axial ratio versus frequency for (a) the RHCP GMM unit-cell element (case 1) and (b) the LHCP GMM unit-cell element (case 2).

III. Reconfigurable Polarization Slot Antenna Using a Graphene-Based Metamaterial Array

The proposed GMM unit-cell element is then arranged in a 4 x 4 array to perform polarization conversion for a linear polarized slot antenna. The proposed LP slot antenna consists of a square PEC sheet of a side length L_{ps} = 119.82 µm with a rectangular slot of length L_s = 62.6 µm and width of W_s = 6 µm. The PEC sheet with the rectangular slot is placed over a square substrate of the same side length, height of H_s= 2.5 µm, and relative permittivity ε_{rs} = 3.38 as shown in Fig. 8. a. The slot antenna is radiated through a strip line which is placed at the bottom of the substate with length L_{st} = 96.5 µm and width W_{st} = 6.5 µm as shown in Fig. 8. b.

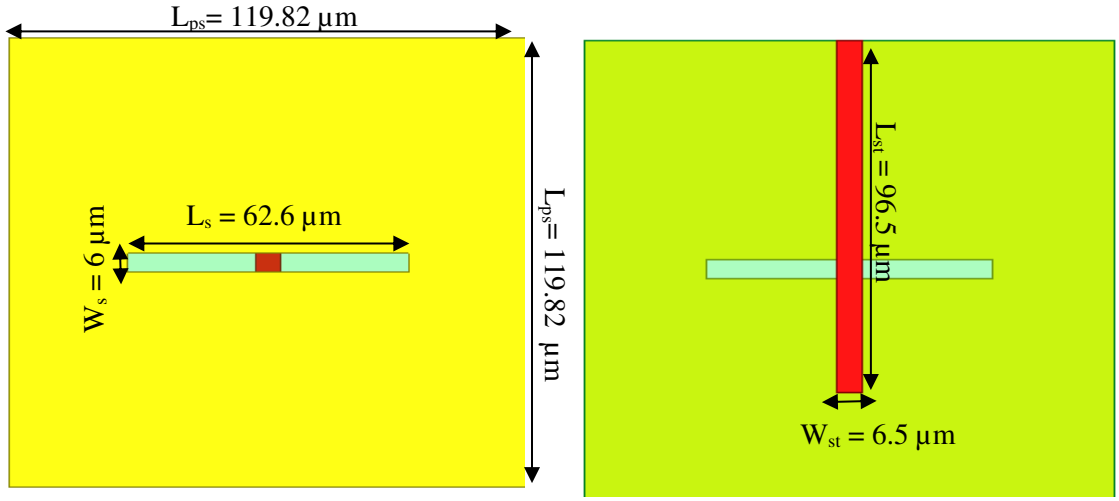

a. b.

Figure 8. (a) The top-view and (b) the bottom-view of the LP slot antenna.

An array of 4 x 4 GMM unit-cell elements with the surface area of 119.82 x 119.82 µm^2 is used as a polarization converter for the proposed slot antenna, as shown in Fig. 9. a. This array is placed under the proposed dipole antenna at an optimized distance h = 25 µm which is equivalent to $\lambda/4$. The reflected wave from the MM array is of a high gain of maximum value 6.18 dBi along the positive z-axis, as shown in Fig.

10. b, with a wide bandwidth from 1.5 THz to 2.1 THz (30.93% -10 dB BW) as shown in Fig. 11. a. It can be noted that the -10 dB BW and the gain of the proposed dipole antenna are greatly enhanced.

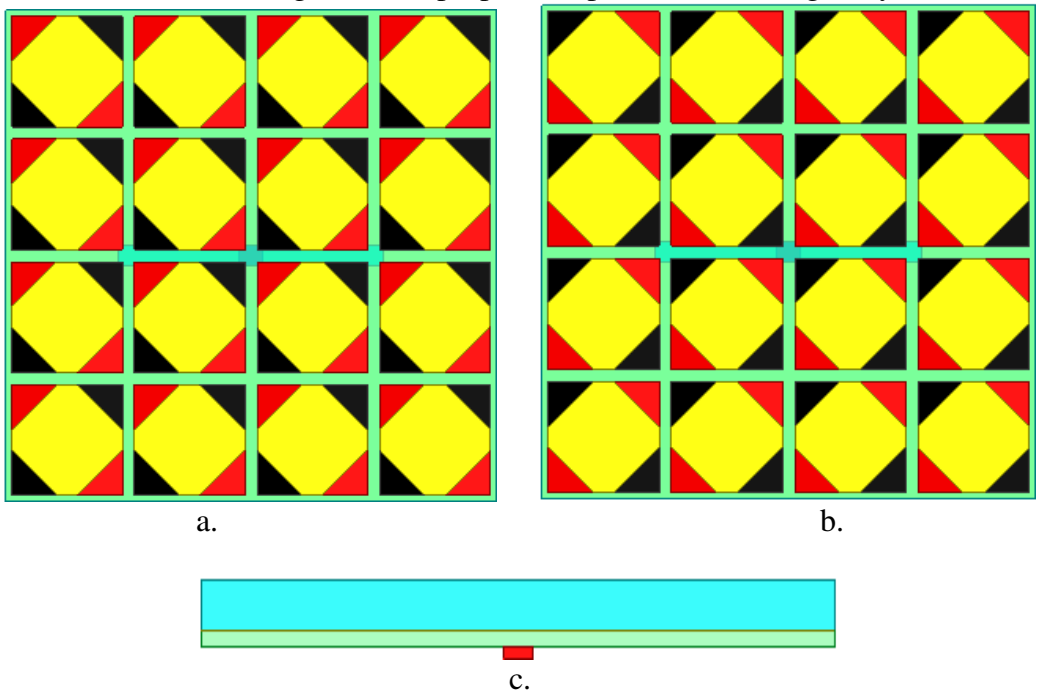

a. b. c.

Figure 9. 4 × 4 GMM unit-cell elements array over the proposed slot antenna for graphene biasing state as in (a) case 1, (b) case 2, and (c) is the side view of the overall construction.

Figure 10. a. shows that the reflection coefficient of the overall construction is enhanced to -22 dB instead of -2 dB of the slot antenna when the graphene triangles are biased as in case 1 and enhanced to -44 dB when the graphene triangles are biased as in case 1 as shown in Fig. 10. b. Moreover, the transmitted wave from the GMM array is converted to RHCP and LHCP waves for case 1 and case 2 respectively as shown in Fig. 11 and Fig. 12.

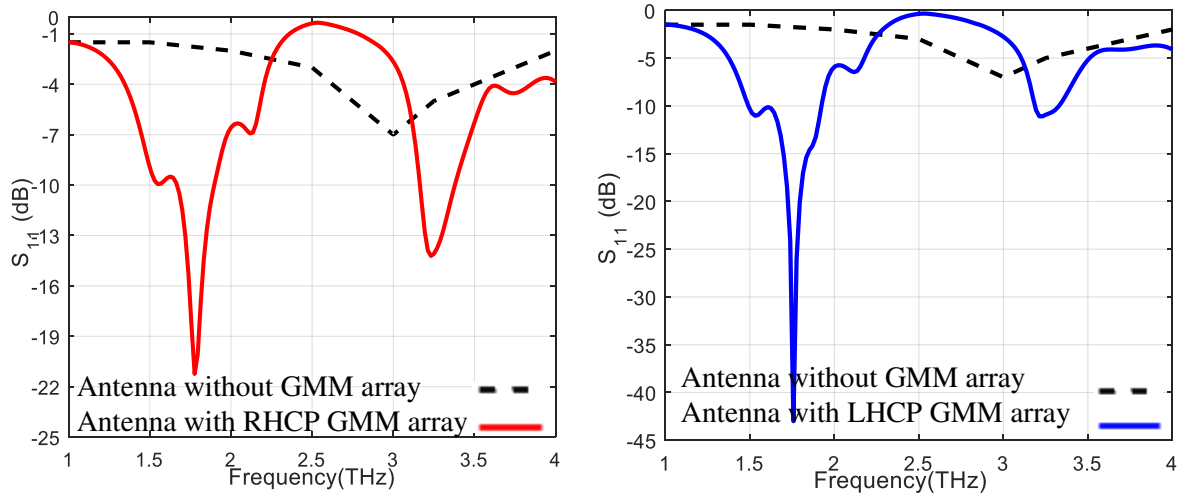

a. b.

Figure 10. The variations of the reflection coefficient versus frequency for the slot antenna against that of the overall construction with biased GMM array (a) case 1 and (b) case 2.

The LP wave of the slot antenna is converted to RHCP wave when the graphene of the GMM array is biased according to case 1. This is confirmed by the results of Fig 11. a, where a wide 3dB-BW of 10.55 %

and ranging from 1.74 THz to 1.93 THz is achieved. Also, the ERHCP component of the radiated field is greater than the ELHCP component by 18 dB at the operating frequency of 1.18 THz as shown in Fig. 12. a. Biasing the graphene of the GMM array according to case 2 produces a LHCP wave with 3dB-AR bandwidth of 13.3 % ranging from 1.73 THz to 1.96 THz as shown in Fig. 11. b. The difference between the ERHCP and LHCP components of the radiated field for this case is 19 dB at the operating frequency of 1.8 THz as shown in Fig. 12. b.

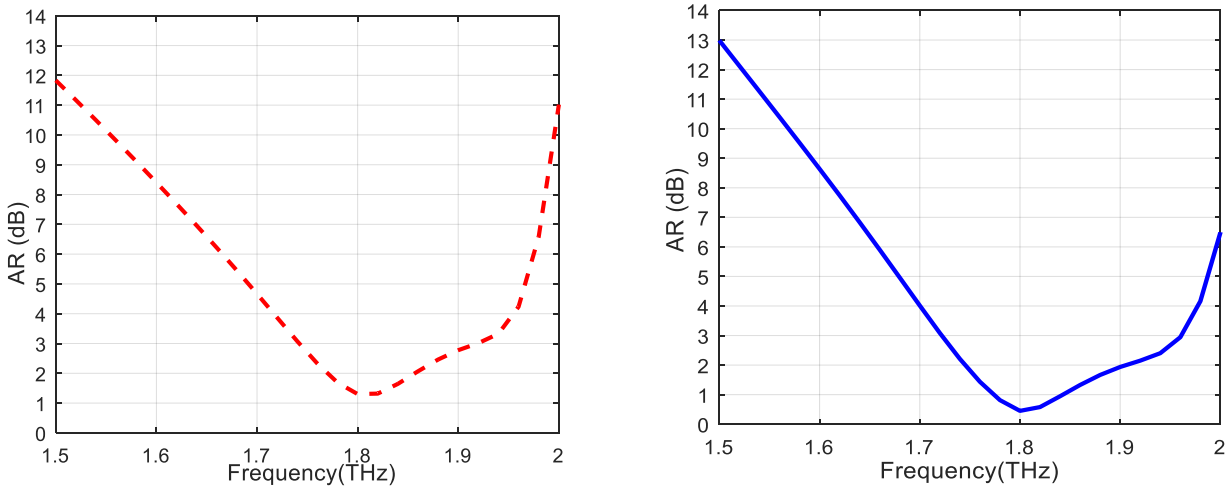

a. b.

Figure 11. The AR of the overall construction with biased GMM array (a) case 1 and (b) case 2.

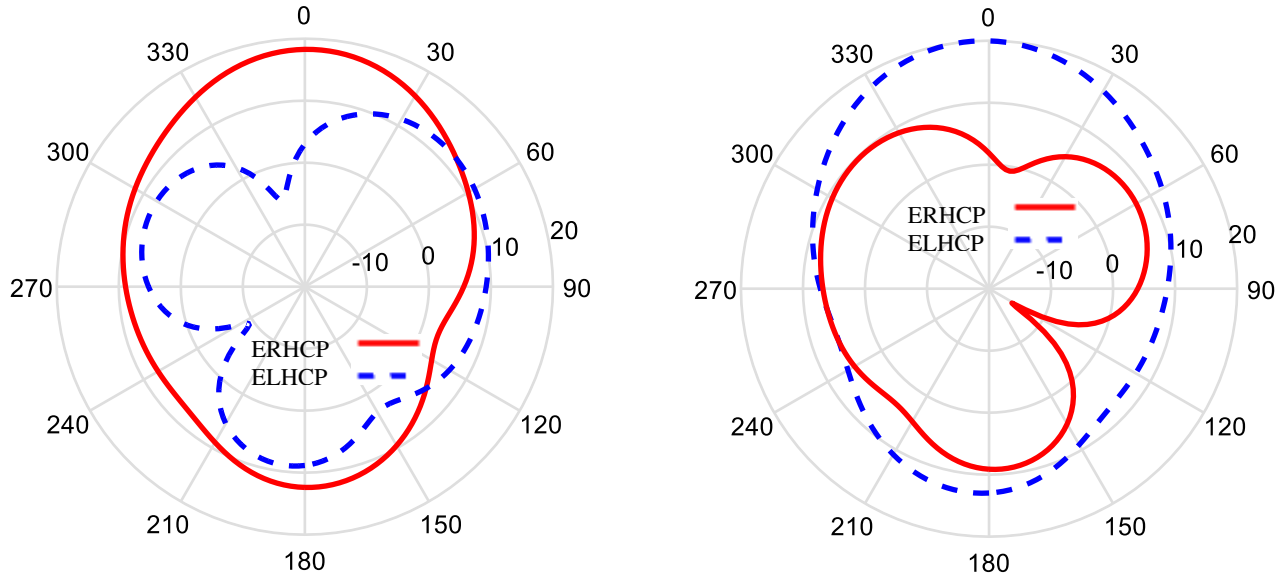

a. b.

Figure 12. The E_R and the E_L of the overall construction with biased GMM array (a) case 1 and (b) case 2.

Compared to similar previous works [29-30], the proposed configuration exhibits an electrical polarization conversion with wider bandwidth, better CP conversion, more simplicity, and wide 3dB-AR bandwidth.

IV. CONCLUSIONS

A graphene-based metamaterial unit-cell element is designed and analysed in this paper at 1.8 THz. A high gain with reconfigurable polarization antenna is introduced using a GMM array. The GMM array consisted of 20 GMM unit-cell elements arranged over the proposed slot antenna. Using the GMM array increased the -10 dB B.W to 22.2 % and the gain of the proposed slot antenna enhanced to 8 dBi instead of

5.8 dBi. Moreover, the GMM polarization converter switched the LP wave from the slot antenna between RHCP and LHCP waves according to its biasing states of the graphene material in two cases 1 and 2 with high 3dB AR bandwidth (10.55 % and 13.3 %, respectively).

REFERENCES

[1] P. Mukherjee and B. Gupta, “Terahertz (THz) frequency sources and antennas-A brief review,” Int. J. Infrared Millimeter Waves, vol. 29, no. 12, pp. 1091–1102, 2008.

[2] M. Tamagnone, J. S. Gómez-Díaz, J. Perruisseau-Carrier, and J. R. Mosig, “Analysis and design of terahertz antennas based on plasmonic resonant graphene sheets,” J. Appl. Phys., vol. 112, no. 11, pp. 114915–1149154, doi: DOI:101063/14768840.

[3] S. D. Keller, A. I. Zaghloul, V. Shanov, M. J. Schulz, D. B. Mast, and N. T. Alvarez, “Electromagnetic Simulation and Measurement of Carbon Nanotube Thread Dipole Antennas,” IEEE Trans. Nanotechnol., vol. 13, no. 2, pp. 394–403, 2014, doi: 10.1109/TNANO.2014.2306330.

[4] D. Yi and X. Wei, “Recent developments of tunable microwave absorbers using graphene,” in 2017 Sixth Asia-Pacific Conference on Antennas and Propagation (APCAP), 2017, pp. 1–3, doi: 10.1109/APCAP.2017.8420527.

[5] N. Sharma, R. Dev Gupta, R. Chandmal Sharma, S. Dayal, and A. Singh Yadav, “Graphene: An overview of its characteristics and applications,” Mater. Today Proc., 2021.

[6] Y. Obeng and P. Srinivasan, “Graphene: Is It the Future for Semiconductors? An Overview of the Material, Devices, and Applications,” Interface Mag., vol. 20, no. 1, pp. 47–52, 2011.

[7] N. Haider, D. Caratelli, and A. G. Yarovoy, "*Recent Developments in Reconfigurable and Multiband Antenna Technology*," International Journal of Antennas and Propagation, vol. 2013, p. 869170, 2013/03/13 2013.

[8] A. Priya, S. Kaja Mohideen, and M. Saravanan, "*Multi-State Reconfigurable Antenna for Wireless Communications*," Journal of Electrical Engineering & Technology, vol. 15, no. 1, pp. 251-258, 2020/01/01 2020.

[9] N. Ojaroudi Parchin, H. Jahanbakhsh Basherlou, Y. I. A. Al-Yasir, A. M. Abdulkhaleq, and R. A. Abd-Alhameed, "*Reconfigurable Antennas: Switching Techniques—A Survey*," vol. 9, no. 2, p. 336, 2020.

[10] J. Costantine, Y. Tawk, and C. G. Christodoulou, "*Reconfigurable antennasReconfigurable Antennas and Their Applications*," in Handbook of Antenna Technologies, Z. N. Chen, Ed. Singapore: Springer Singapore, 2014, pp. 1-30.

[11] M. S. Shakhirul, M. Jusoh, Y. S. Lee, and C. R. Nurol Husna, "*A Review of Reconfigurable Frequency Switching Technique on Micostrip Antenna*," Journal of Physics: Conference Series, vol. 1019, p. 012042, 2018/06 2018.

[12] J. Costantine, Y. Tawk, S. E. Barbin and C. G. Christodoulou, "*Reconfigurable Antennas: Design and Applications*," in Proceedings of the IEEE, vol. 103, no. 3, pp. 424-437, March 2015, doi: 10.1109/JPROC.2015.2396000.

[13] S. Khan and T. F. Eibert, "*A Dual-Band Metasheet for Asymmetric Microwave Transmission With Polarization Conversion*," in IEEE Access, vol. 7, pp. 98045-98052, 2019, doi: 10.1109/ACCESS.2019.2929115.

[14] B. Lin, L. Lv, J. Guo, Z. Liu, X. Ji and J. Wu, "*An Ultra-Wideband Reflective Linear-to-Circular Polarization Converter Based on Anisotropic Metasurface*," in IEEE Access, vol. 8, pp. 82732-82740, 2020, doi: 10.1109/ACCESS.2020.2988058.

[15] Y. Qi, B. Zhang, C. Liu and X. Deng, "*Ultra-Broadband Polarization Conversion Meta-Surface and its Application in Polarization Converter and RCS Reduction*," in IEEE Access, vol. 8, pp. 116675-116684, 2020, doi: 10.1109/ACCESS.2020.3004127.

[16] A. K. Fahad et al., "*Ultra-Thin Metasheet for Dual-Wide-Band Linear to Circular Polarization Conversion With Wide-Angle Performance*," in IEEE Access, vol. 8, pp. 163244-163254, 2020, doi: 10.1109/ACCESS.2020.3021425.

[17] A. K. Baghel, S. S. Kulkarni and S. K. Nayak, "*Linear-to-Cross-Polarization Transmission Converter Using Ultrathin and Smaller Periodicity Metasurface*," in IEEE Antennas and Wireless Propagation Letters, vol. 18, no. 7, pp. 1433-1437, July 2019, doi: 10.1109/LAWP.2019.2919423.

[18] Z. Tao, H. Zhang, H. Xu and Q. Chen, "*Novel Polarization Conversion Metasurface Based Circular Polarized Slot Antenna with Low Profile*," 2019 Cross Strait Quad-Regional Radio Science and Wireless Technology Conference (CSQRWC), Taiyuan, China, 2019, pp. 1-3, doi: 10.1109/CSQRWC.2019.8799106.

[19] Q. Chen and H. Zhang, "*Dual-Patch Polarization Conversion Metasurface-Based Wideband Circular Polarization Slot Antenna*," in IEEE Access, vol. 6, pp. 74772-74777, 2018, doi: 0.1109/ACCESS.2018.2883992.

[20] Y. Li, H. Zhang, T. Yang, T. Sun and L. Zeng, "*A Multifunctional Polarization Converter Base on the Solid-State Plasma Metasurface*," in IEEE Journal of Quantum Electronics, vol. 56, no. 2, pp. 1-7, April 2020, Art no. 7300107, doi: 10.1109/JQE.2020.2975019.

[21] Y. Liu, Y. Hao, K. Li and S. Gong, "*Radar Cross Section Reduction of a Microstrip Antenna Based on Polarization Conversion Metamaterial*," in IEEE Antennas and Wireless Propagation Letters, vol. 15, pp. 80-83, 2016, doi: 10.1109/LAWP.2015.2430363.

[22] H. A. E.-A. Malhat, A. M. Mabrouk, H. El-Hmaily, H. F. Hamed, S. H. Zainud-Deen, and A. A. E. M. Ibrahim, "*Electronic beam switching using graphene artificial magnetic conductor surfaces*," Optical and Quantum Electronics, vol. 52, no. 7, p. 357, 2020/07/14 2020.

[23] A. M. Mabrouk, H. A. Malhat, and S. H. Zainud-Deen, "*Electronic Beam Switching Using Graphene-Based Frequency Selective Surface*," in 2019 36th National Radio Science Conference (NRSC), 2019, pp. 68-75: IEEE.

[24] S. H. Zainud-Deen, A. M. Mabrouk, and H. A. Malhat, "*Terahertz graphene-based metamaterial transmitarray*," Wirel. Pers. Commun., vol. 100, no. 3, pp. 1235-1248, 2018.

[25] Y. Meng, J. Wang, H. Chen, L. Zheng, H. Ma and S. Qu, "*Countering Single-Polarization Radar Based on Polarization Conversion Metamaterial*," in IEEE Access, vol. 8, pp. 206783-206789, 2020, doi: 10.1109/ACCESS.2020.3034927.
[26] S. H. Zainud-Deen, A. M. Mabrouk, and H. A. Malhat, "*Frequency tunable graphene metamaterial reflectarray for terahertz applications*," Wirel. Pers. Commun., vol. 2018, no. 9, pp. 753-761, 2018.
[27] Z. Yang et al., "*Reconfigurable Multifunction Polarization Converter Integrated with PIN Diode*," in IEEE Microwave and Wireless Components Letters, doi: 10.1109/LMWC.2021.3064039.
[28] X. Hu and J. Wang, "Design of graphene-based polarization-insensitive optical modulator," Nanophotonics, vol. 7, no. 3, pp. 651–658, 2018, doi: doi:10.1515/nanoph-2017-0088.
[29] X. Zhang, C. Chen, S. Jiang, Y. Wang, and W. J. P. I. E. R. Chen, "*A High-Gain Polarization Reconfigurable Antenna Using Polarization Conversion Metasurface*," vol. 105, pp. 1-10, 2020.
[30] M. A. Sofi, K. Saurav, and S. K. Koul, "Reconfigurable Polarization Converter Printed on Single Substrate Layer Frequency Selective Surface," in 2019 IEEE MTT-S International Microwave and RF Conference (IMARC), 2019, pp. 1-4: IEEE.